Materials Science & Engineering C 118 (2021) 111443

Contents lists available at ScienceDirect

Materials Science & Engineering C

journal homepage: www.elsevier.com/locate/msec

Hetero-structured MnO-Mn_3O_4@rGO composites: Synthesis and nonenzymatic detection of H_2O_2

Yuanyuan Li[a,b], Li Tang[b], Dongmei Deng[b,*], Haibo He[b], Xiaoxia Yan[b], Jinhua Wang[a,*], Liqiang Luo[b,*]

[a] School of Environmental and Chemical Engineering, Shanghai University, Shanghai 200444, PR China
[b] College of Sciences, Shanghai University, Shanghai 200444, PR China

ARTICLE INFO

Keywords:
Hetero-structured
MnO-Mn_3O_4@rGO
H_2O_2
Electroreduction

ABSTRACT

The construction of metal-oxide heterojunction architecture has greatly widened applications in the fields of optoelectronics, energy conversions and electrochemical sensors. In this study, olive-like hetero-structured MnO-Mn_3O_4 microparticles wrapped by reduced graphene oxide (MnO-Mn_3O_4@rGO) were synthesized through a facile solvothermal-calcination treatment. The morphology and structure of MnO-Mn_3O_4@rGO were characterized by scanning electron microscopy, transmission electron microscopy, X-ray photoelectron spectroscopy, Raman spectroscopy, and X-ray diffraction. The as-synthesized MnO-Mn_3O_4@rGO exhibited prominent catalyzing effect on the electroreduction of H_2O_2, due to the combination of good electrical conductivity of rGO and the synergistic effect of MnO and Mn_3O_4. The MnO-Mn_3O_4@rGO modified glassy carbon electrode provided a wide linear response from 0.004 to 17 mM, a low detection limit of 0.1 μM, and high sensitivity of 274.15 μA mM^{-1} cm^{-2}. The proposed sensor displayed noticeable selectivity and long-term stability. In addition, the biosensor has been successfully applied for detecting H_2O_2 in tomato sauce with good recovery, revealing its promising potential applications for practical electrochemical sensors.

1. Introduction

In the past decades, transition metal oxides have become a research hotspot due to their unusual electronic and magnetic properties, facile fabrication and good catalytic performance. Especially in the field of electrochemical sensing, numerous transition metal oxides (MnO_2, NiO, CoO_x, FeO_x, CuO, etc.) have been served as enzyme mimics due to their diverse morphology, high theoretical capacity and good mechanical behavior [1–6]. Among them, manganese oxides (MnO_2, MnO and Mn_3O_4) have found increasing application in biochemical sensors because of their natural abundance, environmental compatibility and affordable cost [7–10]. For instance, Zhu et al. [11] synthesized Au/MnO nanoparticles by regulating the oxidizing process of AuMn, which exhibited great performance for the electrochemical reduction of H_2O_2 with a detection limit of 8 nM. Wang et al. [12] synthesized Mn_3O_4 octahedron sub-microstructures by solvothermal method for the nonenzymatic detection of H_2O_2. Song et al. [13] fabricated a hollow urchin-like MnO_2 by hydrothermal technique for the electrochemical detection of H_2O_2 and dopamine. Thus, nano/micro-architectured manganese oxides with multiple valence states have gained wide attention in electrochemical sensors. However, MnO_x has poor electrical conductivity, resulting in low selectivity and sensitivity for the determination of H_2O_2 [14].

Recently, heterojunction materials with desired morphologies and wonderful synergistic effects have attracted considerable attention [15–19]. Especially, the hetero-composites based on transition metal oxides have potential applications in catalysis owing to their reversible mixed-valence states and more surface active sites [18,20–22]. For example, Bera et al. [18] constructed Pt loaded Bi_2O_3-ZnO heterojunction, and the material showed good catalytic performance for the electrooxidation of methanol due to their enhanced synergic catalytic activity. Praveen et al. [20] synthesized the hetero-nanostructured Cu_2O-Au nanocomposite. Benefited from their strong interaction, the Cu_2O-Au modified electrode showed high electrocatalytic activity towards glucose. Asif et al. [23] designed a new type of p-n heterojunction MnAl layered double hydroxide wrapped CuO nanospheres as an efficient electrocatalyst towards H_2O_2 reduction. Therefore, hetero-structured materials have demonstrated significant improvements for electrochemical sensors.

Hydrogen peroxide (H_2O_2), an oxidizing agent, is critical to

* Corresponding authors.
E-mail addresses: dmdeng@shu.edu.cn (D. Deng), jinhuawang@shu.edu.cn (J. Wang), luck@shu.edu.cn (L. Luo).

https://doi.org/10.1016/j.msec.2020.111443
Received 25 February 2020; Received in revised form 10 August 2020; Accepted 20 August 2020
Available online 26 August 2020
0928-4931/

biological, chemical, and pharmaceutical systems [24–26]. Commonly, H_2O_2 has been employed as a food additive to regulate the growth of microorganisms in stored food such as fruit juice, dried fruit, ketchup and milk to avoid food spoilage [27–29]. Nevertheless, oxidative stress and cellular damage will be induced by long-time exposure to high concentration of H_2O_2. Accordingly, neurodegenerative disorders, bleeding in mucous membrane, ulceration and cancer will be triggered [29–32].

Graphene is considered as a fascinating candidate support for electrocatalysts because of its robust two-dimensional honeycomb lattice structure, high conductivity (10^3–10^4 S m^{-1}) and large surface area of (2630 m^2 g^{-1}) [33–35]. Compared to graphene, its oxygen derivative, reduced graphene oxide (rGO) has been paid more attention for its easy design and unique features, including high electron mobility (2.0×10^5 cm^2 V^{-1} s^{-1}), good chemical stability and biocompatibility [36]. In recent years, rGO has found extensive application as electrode modifiers in the electrochemical field. Previous studies have confirmed that the introduction of rGO to transition mental oxide can make electrode materials more conductive, thereby improving the electrochemical performance of the biosensor [37]. For instance, Mahmoudian et al. [38] reported the fabrication of MnO_2 nanotubes/rGO nanocomposite by hydrothermal technique and used as the catalyst for the detection of H_2O_2. Wang et al. [39] synthesized binary ZnO-CoO nanoparticles loaded on rGO, and the ZnO-CoO/rGO electrode can detect both glucose and H_2O_2. Wang et al. [40] constructed ZnO-SnO_2 heterostructure on rGO to enhance NO_2 sensing performance. Therefore, it would be an ideal strategy to assemble rGO-based heterostructured composites with controlled morphology and improved catalytic ability. To the best of our knowledge, no work has been reported to synthesize hetero-structured MnO-Mn_3O_4@rGO as electrocatalyst for electrochemical sensing of H_2O_2.

Herein, we demonstrated a facile solvothermal-calcination treatment to synthesize hetero-structured MnO-Mn_3O_4@rGO (Fig. 1). Taking advantages of the strong synergistic effect of heterojunction and excellent conductivity of rGO, the synthesized MnO-Mn_3O_4@rGO exhibited efficient electrocatalytic activity towards H_2O_2 reduction. The proposed MnO-Mn_3O_4@rGO modified glassy carbon electrode (GCE) displayed excellent selectivity, sensitivity and stability. Moreover, the as-prepared sensor was applied to detect H_2O_2 in tomato sauce.

2. Experimental

2.1. Apparatus

The morphology of the samples was analyzed under a scanning electron microscopy (SEM, JSM-6700F, Japan) with energy dispersive spectroscopy (EDS) at 200 kV. The details of the crystal structure were further characterized by transmission electron microscopy (TEM) on JEM-200CX operating at 200 kV. X-ray diffraction (XRD) was conducted on Rigaku DLMAX-2200 (Cu Kα radiation, λ = 1.5418 Å, 40 mA, working voltage: 40 kV, scanning rate: 0.08° s^{-1}). X-ray photoelectron spectroscopy (XPS) was conducted on an ESCA commercial device (Sigma Probe, Thermo VG-Scientific) with an Al Kα radiation source (1486.6 eV). Raman spectra were conducted on Renishaw (INVIA, England) in the spectral range of 200–1000 nm (spectral resolution: 1 cm^{-1}). Electrochemical measurements were carried out on a CHI 660D electrochemical workstation (Shanghai CH Instruments, China) with a traditional three-electrode cell, in which a modified GCE, Ag/AgCl (saturated KCl) and a platinum foil were used as working, reference and counter electrodes, separately.

2.2. Chemicals

$MnCl_2{\cdot}4H_2O$, NaOH, $(CH_2OH)_2$, $CO(NH_2)_2$ and H_2O_2 were obtained from Sinopharm Reagent (Shanghai, China). Aladdin Reagent (Shanghai, China) provided graphene oxide (GO). Glycocoll (Gly), citric acid (CA), dopamine (DA), citric acid (AA), uric acid (UA), glucose (Glu) were purchased from Sigma (USA). All chemicals were of analytical grade. Milli-Q water (18.25 MΩ cm) was employed during experimental process.

2.3. Synthesis of MnO-Mn_3O_4@rGO composites

MnO-Mn_3O_4@rGO composites were synthesized with solvothermal-calcination method following the literature procedure with some modification [41]. Firstly, GO dispersion (1 mg ml^{-1}) was prepared by adding GO in 80 ml ethylene glycol and ultrasonicating for 40 min. Then, 0.792 g $MnCl_2{\cdot}4H_2O$ was added in the dispersion and dispersed evenly by ultra-sonication for another 30 min. Subsequently, 0.6 g urea was introduced to the above solution followed with vigorously stirring for 40 min. Next, the light red mixture was transferred into a 100 ml Teflon-lined autoclave. After being heated at 200 °C for 24 h, the resulting solution was collected and washed with anhydrous ethanol and water repeatedly, followed by vacuum drying overnight at 60 °C. Lastly, the resultant precursor underwent calcining process at 400 °C, 500 °C and 600 °C for 1 h in N_2 atmosphere to produce MnO-Mn_3O_4@rGO composites. In contrast, under identical conditions, MnO-Mn_3O_4 microspheres without GO were synthesized. At the same time, the precursor powder calcined at 500 °C for 1 h in air was also processed. The synthesis process is illustrated in Fig. 1.

2.4. Preparation of the modified electrode

The preparation process of the modified electrode was similar to our previous work [42]. With the Buehler polishing kit, GCE (with a diameter of 3 mm) underwent polishing with alumina powder of 0.05 and 0.3 μm carefully. Then, the GCE was ultrasonically treated in Milli-Q water and alcohol separately for 3 min. After removing any adherent impurities on its surface, GCE was dried at room temperature.

Next, a certain amount of MnO-Mn_3O_4@rGO composites was introduced into water and underwent sonication for 30 min. 5 μl of the resulting MnO-Mn_3O_4@rGO dispersion was dropped on surface of the

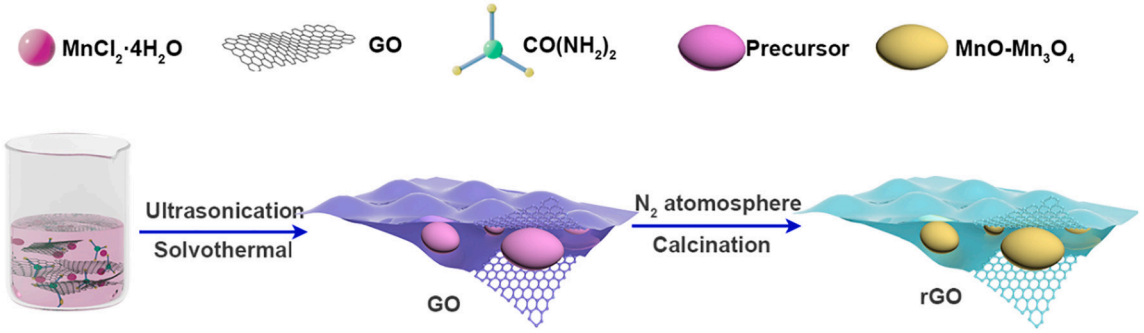

Fig. 1. Schematic diagram of the major steps for the synthesis of MnO-Mn_3O_4@rGO.

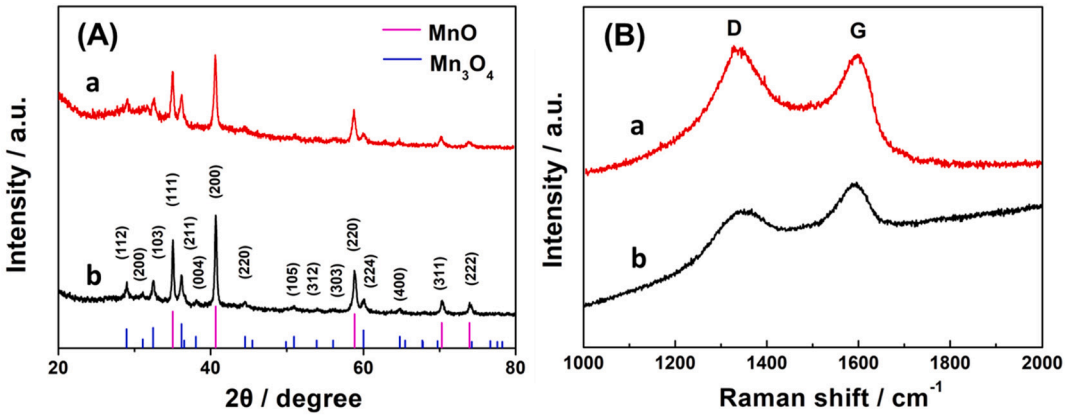

Fig. 2. (A) XRD pattern of MnO-Mn_3O_4@rGO (curve a) and MnO-Mn_3O_4 (curve b); (B) Raman spectra of MnO-Mn_3O_4@rGO (curve a) and GO (curve b).

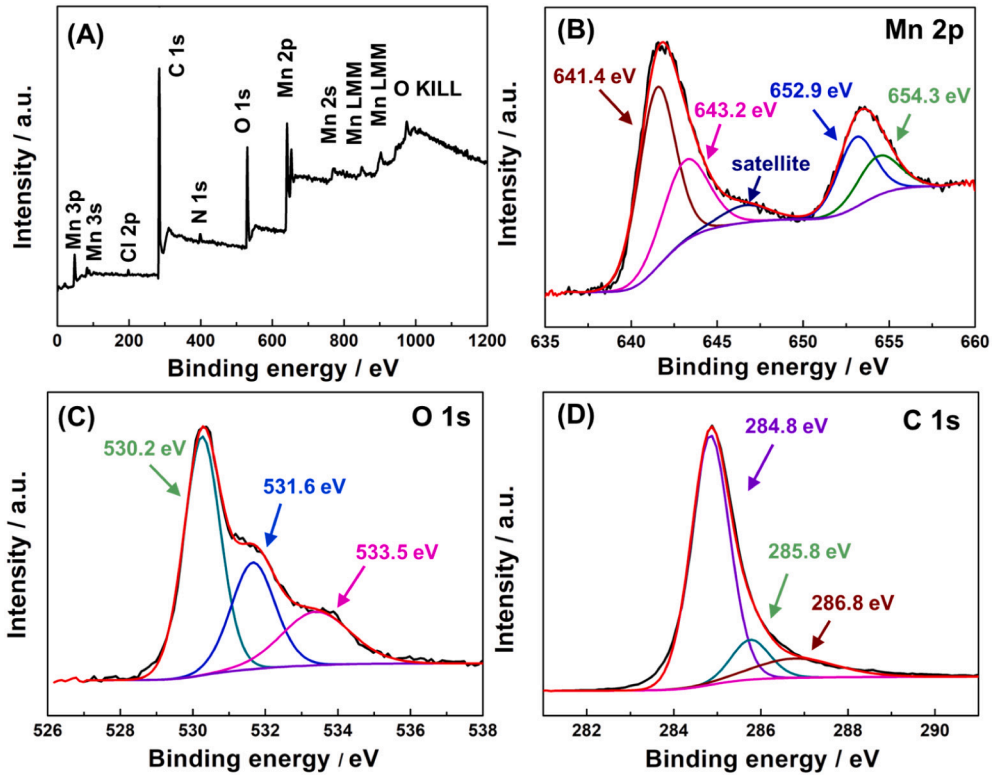

Fig. 3. XPS spectra of MnO-Mn_3O_4@rGO: (A) full wide-scan, (B) Mn 2p, (C) O 1 s, and (D) C 1 s.

pretreated GCE, and then dried under the infrared lamp for 5 min to fabricate MnO-Mn_3O_4@rGO/GCE.

2.5. Real sample preparation

The developed H_2O_2 sensor based on enzyme mimics MnO-Mn_3O_4@rGO was assessed by determining H_2O_2 in tomato sauce. Before electrochemical measurement, the sample of tomato sauce was pretreated according to previously described method [43]. Briefly, 1 g of tomato sauce was dissolved in 100 ml water to make homogeneous suspension under sonication. Then, the homogeneous suspension underwent centrifugation for 10 min at 6000 rpm to produce a clear solution. The amperometric detection was performed under the optimal condition with 10 μl pretreated sample injected.

3. Results and discussion

3.1. XRD, Raman and XPS spectroscopy characterization

In our work, hetero-structured MnO-Mn_3O_4@rGO composites were synthesized by a solvothermal-calcination method. The ambient atmosphere and temperature in the calcination process were the major controlling factors. When calcination temperature was set at 400 ˚C in N_2, the diffraction peaks of $MnCO_3$ still existed in the product (Fig. S1A). XRD patterns of MnO-Mn_3O_4 and MnO-Mn_3O_4@rGO at 500 ˚C in N_2 are shown in Fig. 2A. The peaks at 28.9˚, 32.3˚, 36.0˚ and 44.4˚ can be assigned to the (112), (103), (211) and (220) crystal planes of the tetragonal Mn_3O_4 phase (JCDPS, card no. 24–0734), while the robust diffraction peaks at 58.7˚, 40.5˚, and 34.9˚ can be indexed to the (220), (200), and (111) planes of face-centered cubic MnO phase (JCDPS, card no. 07–0230) [44]. The MnO-Mn_3O_4@rGO composites show similar diffraction peaks to the MnO-Mn_3O_4, suggesting that the addition of

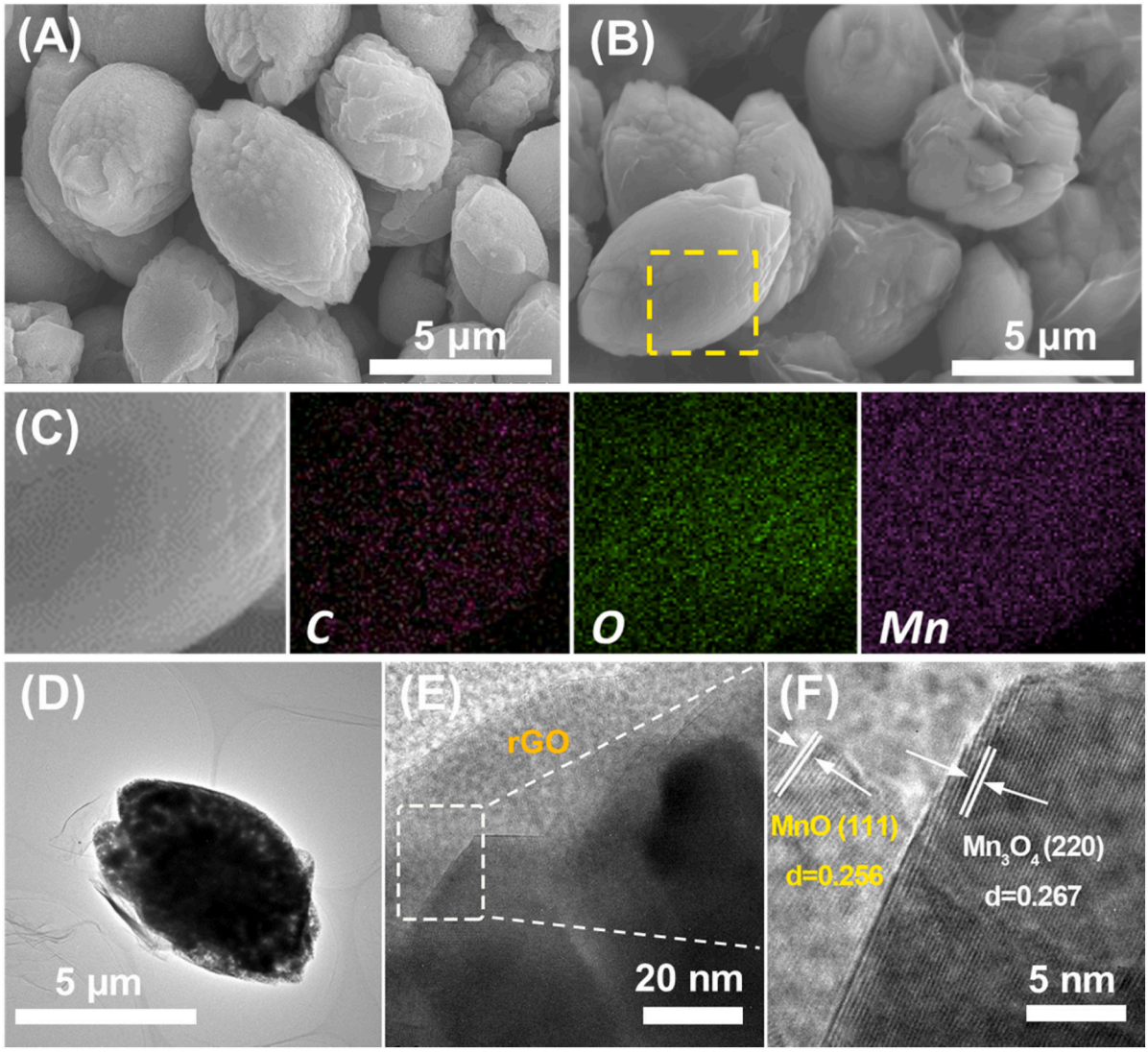

Fig. 4. (A) SEM image of MnO-Mn_3O_4; (B) SEM image of MnO-Mn_3O_4@rGO; (C) Elemental mapping images of MnO-Mn_3O_4@rGO in the area indicated by the yellow rectangular in (B); (D) TEM image; (E, F) The high-resolution TEM images. (For interpretation of the references to colour in this figure legend, the reader is referred to the web version of this article.)

rGO did not affect the formation of hetero-structured MnO-Mn_3O_4. The XRD pattern of the precursor powder calcined at 500 °C in air is shown in Fig. S1B. All the diffraction peaks are indexed to the lattice planes of Mn_2O_3 (JCPDS card no. 41–1442). Therefore, when the precursor was calcined in air, only Mn_2O_3 could be obtained. As indicated in Raman spectroscopy (Fig. 2B), the two peaks at 1598 and 1328 cm^{-1} represent the G and D bands of rGO, separately [45]. The relevant I_D/I_G ratio of 1.40 is larger than the value of 0.9 for GO. Therefore, it is demonstrated that GO in the composites has been converted to rGO during the calcinating process.

The valence state and chemical composition on the surface of MnO-Mn_3O_4@rGO composites were explored by XPS. From the survey XPS spectrum (Fig. 3A), characteristic peaks of Mn, C, and O can be identified. The slight peaks of N and Cl might result from the residual $MnCl_2$ and urea of raw experimental materials. As shown in Fig. 3B, two significant peaks at binding energies of 641.4 and 652.9 eV are ascribed to Mn $2p_{3/2}$ and Mn $2p_{1/2}$, respectively, which is well in compliance with the results achieved for MnO [46–48]. The peaks at 643.2 and 654.3 eV are from Mn $2p_{3/2}$ and Mn $2p_{1/2}$, respectively, agreeing well with the data of Mn_3O_4 reported previously [49,50]. Besides, the XPS spectrum of Mn 3 s (Fig. S2) with a spin-energy separation of 5.79 eV suggests the presence of MnO [51–53]. The satellite of Mn 2p at 647 eV confirms that the dominant contribution is from MnO [54]. The satellite can be explained as shake-up excitation, originating from the charge-transfer between outer electron shell of ligand and the unfilled 3d shell of MnO during creation of core hole in the photoelectron process [55–57]. The high-resolution O 1 s spectrum can be deconvoluted into three peaks. According to Fig. 3C, the strongest peak at 530.2 eV is consistent with Mn − O. The peak at 531.6 eV corresponds to chemisorbed oxygen surface species, and the peak at 533.5 eV indicates the physisorbed or chemisorbed water [52,58]. The high-resolution C1s spectrum of MnO-Mn_3O_4@rGO in Fig. 3D can be fitted into three peaks at 284.8, 285.8, and 286.8 eV, which are ascribed to C − C, C − OH, and C − O in rGO, separately [59,60]. The percentage data of Mn, O, and C atomics in MnO-Mn_3O_4@rGO are calculated to be 6.93%, 17.37%, 75.7%, respectively. Therefore, the XPS results confirm the successful synthesis of MnO-Mn_3O_4@rGO composites.

3.2. Morphological analysis

Fig. 4A is the SEM image of MnO-Mn_3O_4 composites, which exhibits an olive-like structure with an average diameter of 4 μm. The SEM image of MnO-Mn_3O_4@rGO composites in Fig. 4B shows the same olive-like structure, in which wrinkled rGO sheets well wrap around the

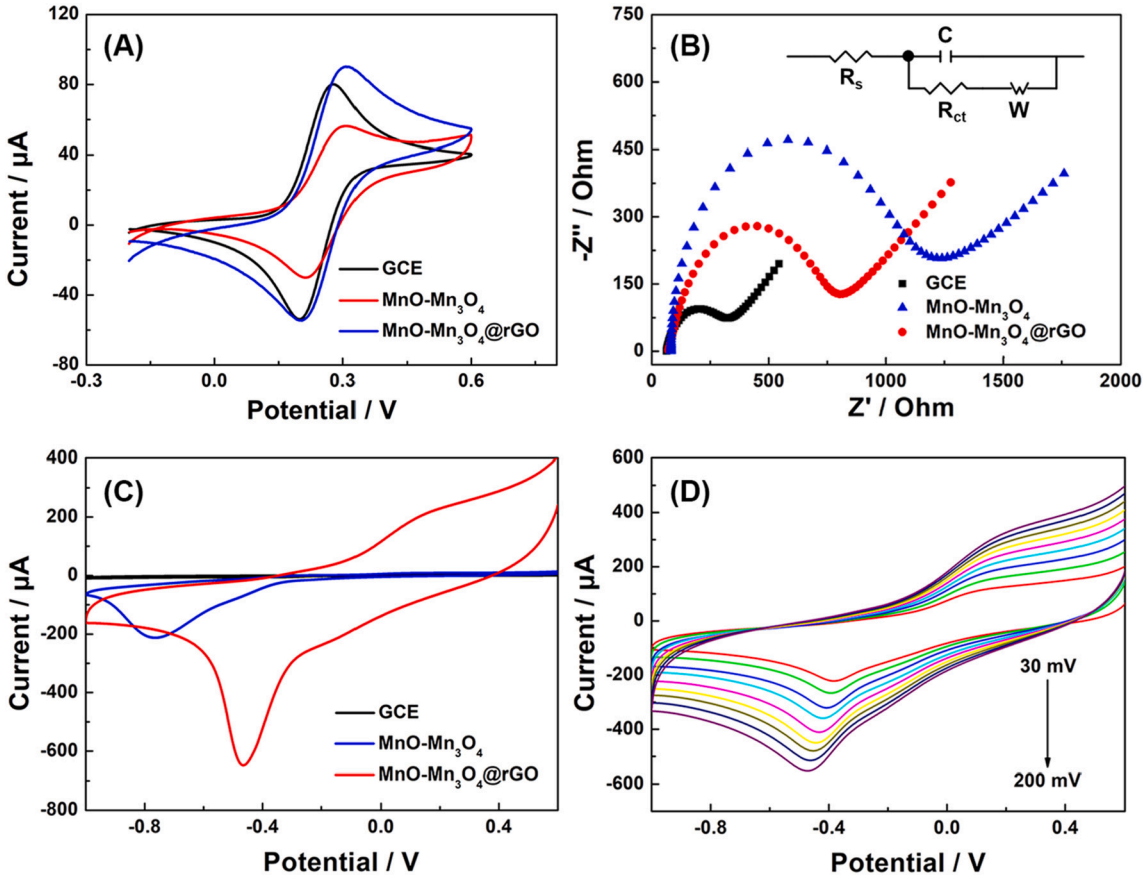

Fig. 5. CVs (A) and EIS (B) recorded in 5.0 mM $[Fe(CN)_6]^{3-/4-}$ + 0.1 M KCl at the GCE, MnO-Mn_3O_4 and MnO-Mn_3O_4@rGO/GCE; (C) CVs of the bare GCE, MnO-Mn_3O_4/GCE and MnO-Mn_3O_4@rGO/GCE in the presence of 4 mM H_2O_2; (D) CVs of MnO-Mn_3O_4@rGO/GCE at different scan rates.

surfaces of MnO-Mn_3O_4. The rGO looks highly transparent with silky appearance, and the introduction of rGO does not change the morphology of the composites. Moreover, rGO keeps the MnO-Mn_3O_4 composites from aggregation, maintaining the high surface area of the composites. Fig. 4C presents the EDS mapping of MnO-Mn_3O_4@rGO composites, clarifying the homogeneous distribution of C, O and Mn elements. Fig. 4D shows the TEM image of MnO-Mn_3O_4@rGO. The olive-like morphology of MnO-Mn_3O_4@rGO can be observed, in which MnO-Mn_3O_4 is tightly wrapped by rGO. The corresponding HRTEM image (taken from the marked area in Fig. 4E) indicates the formation of MnO-Mn_3O_4 heterostructures. As shown in Fig. 4F, the lattice fringes of 0.256 and 0.267 nm are corresponding to MnO (111) and Mn_3O_4 (220), respectively. These results are in accordance with the XRD data, indicating the successful formation of hetero-structured MnO-Mn_3O_4. By comparing the SEM images of the synthesized MnO-Mn_3O_4@rGO composites at 400 and 600 °C, it can be concluded that higher calcination temperature in N_2 would cause the olive-like structure shrunken and broken (Fig. S3A, B). When the calcination process was taken in air, the synthesized MnO-Mn_3O_4@rGO composites were agglomerated into massive blocks, and graphene oxide was burned out in air simultaneously (Fig. S3C). Taking into account of both XRD and SEM, the hetero-structured MnO-Mn_3O_4@rGO composites were synthesized at 500 °C in N_2 atmosphere.

3.3. Electrochemical characterization

Cycle voltammetry (CV) and electrochemical impedance spectroscopy (EIS) were applied in 5.0 mM $[Fe(CN)_6]^{3-/4-}$ + 0.1 M KCl to assess the electrochemical properties of bare GCE, MnO-Mn_3O_4/GCE and MnO-Mn_3O_4@rGO/GCE. As shown in Fig. 5A, a pair of narrow and high redox peak currents was obtained on bare GCE. Compared to bare GCE, lower redox peak currents with a larger potential difference could be observed at MnO-Mn_3O_4/GCE. However, the redox peak currents increased greatly on MnO-Mn_3O_4@rGO/GCE, demonstrating that rGO can enhance the conductivity of the hetero-structured MnO-Mn_3O_4 composites. EIS is an effective way of probing the interfacial properties between the electrode surface and the electrolyte. In this technique, the semicircle diameter at higher frequency indicates electron transfer kinetics occurring on the electrode interface, and the linear portion at a lower frequency corresponds to the diffusion process [61]. The experimental impedance data were fitted with conventional Randles equivalent electrical circuit, including solution resistance (R_s), charge transfer resistance (R_{ct}), double layer capacitance (C), and Warburg impedance (W), as shown in Fig. 5B. The R_{ct} of bare GCE was calculated to be 230 Ω, and the R_{ct} of MnO-Mn_3O_4/GCE increased to 1068 Ω. However, the R_{ct} of MnO-Mn_3O_4@rGO/GCE decreased considerably to 670 Ω, because the introduction of rGO enhanced the conductivity of the MnO-Mn_3O_4. The EIS results are in good agreement with those of CVs.

It has been reported that heterostructure can promote kinetics on the active-sites, improve conductivity, and enhance the electrocatalytic performance [62,63]. CV was performed to assess the electrocatalytic activity of the synthesized MnO-Mn_3O_4@rGO composites towards H_2O_2 reduction by adding 4 mM H_2O_2 in 0.2 M NaOH electrolyte at the scan rate of 100 mV s^{-1}. As shown in Fig. 5C, no current could be observed on bare GCE, while an obvious reduction peak current was obtained at −0.75 V on MnO-Mn_3O_4/GCE. In comparison with bare GCE and MnO-Mn_3O_4/GCE, a noticeable reduction peak current was achieved at −0.45 V on MnO-Mn_3O_4@rGO/GCE, and the overpotential for H_2O_2 electroreduction was lowered about 300 mV. The reason behind this inspiring result can be explained from the following aspects: (i) The multiple valences of manganese can benefit the redox reactions

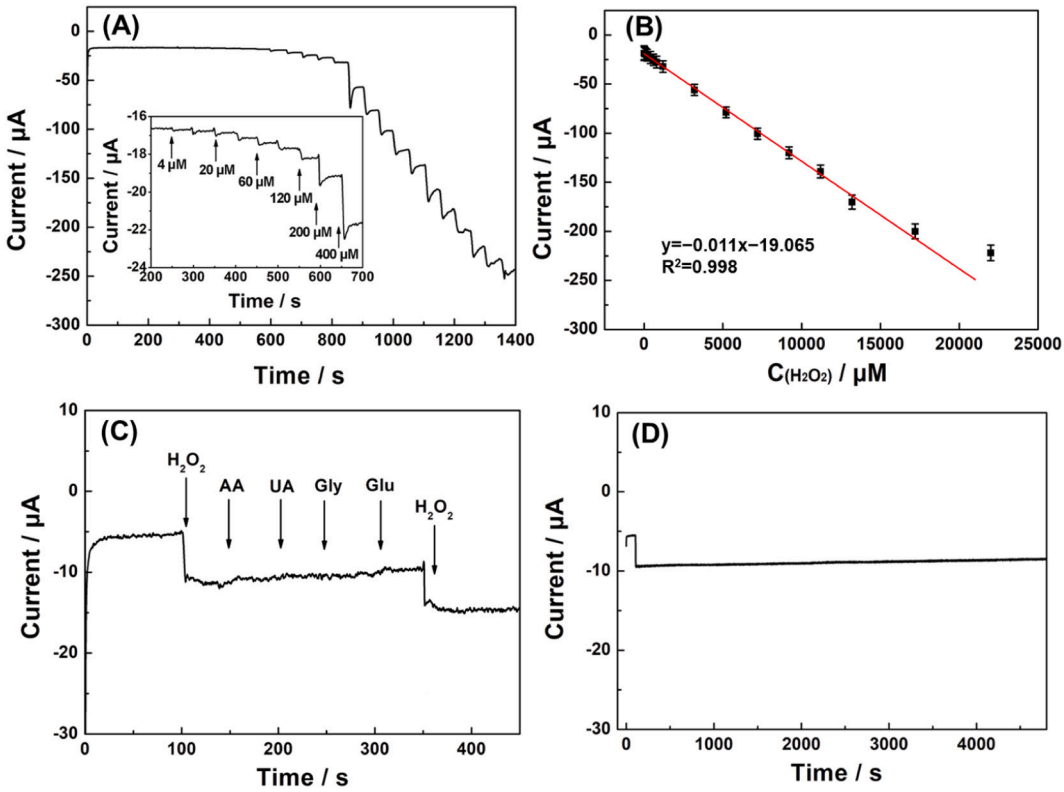

Fig. 6. (A) Amperometric response of MnO-Mn_3O_4@rGO/GCE for different concentrations of H_2O_2 in 0.2 M NaOH at applied potential of −0.45 V; (B) Corresponding calibration curve; (C) Amperometric response of MnO-Mn_3O_4@rGO/GCE to 0.2 mM H_2O_2 and different interferences in stirring 0.2 M NaOH at applied potential of −0.45 V; (D) The stability test of MnO-Mn_3O_4@rGO/GCE over 4800 s.

Table 1
Comparison of property between the proposed sensor and other H_2O_2 sensors.

Modified material	Linear range (μM)	Detection limit (μM)	Reference
Co_3O_4-NWs/CF[a]	10 − 1400	1.4	[65]
Cu_2O/graphene	30–7800	20.8	[66]
Pt-ZnO nanotube	20–5000	1.5	[67]
$NiCo_2S_4$/rGO	25–11,250	0.19	[68]
Pt/Fe_3O_4/rGO	100–2400	1.58	[69]
$CoFe_2O_4$	10–1200	2.5	[70]
NiO/α-Fe_2O_3	500–3000	50	[71]
CuO/PANI[b]	5–9255	0.11	[72]
MnO_2/Co_3O_4/Graphene	5–1200	0.8	[73]
MnO-Mn_3O_4@rGO	4–17,000	0.1	This work

[a] Nanowires/3D N-doped C foam.
[b] Polyaniline.

Table 2
Real sample analysis of MnO-Mn_3O_4@rGO/GCE for the determination of H_2O_2 in tomato sauce samples.

Sample	Added (μM)	Found (μM)	Recovery (%)	RSD (%)
1	50	50.15	100.3	1.81
2	50	50.08	100.16	2.11
3	50	49.81	99.62	1.87
4	50	49.58	99.16	2.02

occurring at electrode material/analyte interface; (ii) The built heterostructure through coupling MnO and Mn_3O_4 with different bandgaps can enhance the surface reaction kinetics and electron transfer, owing to the internal electric field at heterointerfaces [64]; (iii) The introduction of rGO sheets can not only increase the electrical conductivity but also enlarge the active surface area of the catalyst (Scheme S1). The CV responses of MnO-Mn_3O_4@rGO in 4 mM H_2O_2 and 0.2 M NaOH solution from 30 to 200 mV s^{-1} are presented in Fig. 5D. The reduction current rose progressively with the rise of the scan rate. Furthermore, the scan rates keep a linear relation with the currents, suggesting that the reduction of H_2O_2 on the MnO-Mn_3O_4@rGO/GCE can be interpreted as a surface-controlled process (Fig. S4A). In addition, the reduction peak current increased when H_2O_2 was added continuously, proving the catalytic activity of the biosensor to H_2O_2 (Fig. S4B).

3.4. Amperometric detection of H_2O_2 on Mn_3O_4@rGO/GCE

The experimental parameters for the electroreduction of H_2O_2 with MnO-Mn_3O_4@rGO/GCE were optimized, such as the concentration of supporting electrolyte (NaOH), applied potential and the concentration of modifier (Fig. S5). Under optimal conditions (0.2 M NaOH, −0.45 V, and 13.0 mg ml^{-1} MnO-Mn_3O_4@rGO), the typical current-time curve was plotted for MnO-Mn_3O_4@rGO/GCE as H_2O_2 was added at various concentrations (Fig. 6A). Fig. 6B gives the corresponding calibration curve. The current density increases in a linear manner with the increase of H_2O_2 concentration from 0.004 to 17 mM. The sensitivity is calculated to be 274.15 μA mM^{-1} cm^{-2} and the detection limit is 0.1 μM at signal/noise = 3. Compared to other reported H_2O_2 biosensors, the proposed MnO-Mn_3O_4@rGO/GCE exhibited a comparable wide linear range with a lower detection limit (Table 1).

Selectivity is a necessary factor to assess the sensor performance. The selectivity of the MnO-Mn_3O_4@rGO/GCE was explored against common coexisting analytes, such as AA (1-fold), UA (1-fold), Gly (1-fold) and Glu (100-fold). According to the experimental result in Fig. 6C, the MnO-Mn_3O_4@rGO/GCE suggests high selectivity under the low applied potential. The stability of MnO-Mn_3O_4@rGO/GCE was assessed by ascertaining the amperometric current response of MnO-Mn_3O_4@rGO/GCE with 0.2 mM H_2O_2 added. Fig. 6D shows that the

current response remained stable by continuous determination of 0.2 mM H_2O_2 during 4800 s, suggesting that the MnO-Mn_3O_4@rGO/GCE exhibits high stability. Besides, the reusability of the biosensor was tested by using the same modified GCE to detect 1 mM H_2O_2 for seven times in 0.2 M NaOH at the scan rate of 100 mV s^{-1}. As shown in Fig. S6, the relative standard deviation was 2.7%, indicating that MnO-Mn_3O_4@rGO/GCE has good reusability.

3.5. Real sample analysis

The as-prepared sensor was adopted to detect H_2O_2 in tomato sauce. Tomato sauce was purchased from a local supermarket in Shanghai (China), in which H_2O_2 was undetectable by amperometric method. Recovery test was made to validate the feasibility of our proposed sensor. Four samples were evaluated to detect H_2O_2 by standard addition approach. As shown in Table 2, the recoveries were in the range of 99.16–100.30%, and the relative standard deviations (RSDs) were 1.81–2.11%. The results suggest the practical application of the proposed sensor for H_2O_2 detection in real sample.

4. Conclusions

In this study, olive-like hetero-structured MnO-Mn_3O_4@rGO composites have been successfully synthesized by a simple solvothermal-calcination method. The MnO-Mn_3O_4@rGO composites exhibit prominent performance to the electrocatalytic reduction of H_2O_2. The excellent electrical conductivity of rGO and synergetic effect of hetero-structured MnO-Mn_3O_4 greatly enhance the electrocatalytic activity towards H_2O_2 reduction. The as-prepared MnO-Mn_3O_4@rGO/GCE shows good performance to determine H_2O_2 with a wide linear range (0.004–17 mM) and high sensitivity (274.15 μA mM^{-1} cm^{-2}). Furthermore, the proposed biosensor is feasible to determine H_2O_2 in food sample, suggesting promising potential applications of hetero-structured metal oxides composites in electrochemical sensors.

CRediT authorship contribution statement

Yuanyuan Li: Conceptualization, Methodology, Investigation, Writing - original draft, Writing - review & editing. **Li Tang:** Formal analysis, Investigation. **Dongmei Deng:** Investigation, Funding acquisition. **Haibo He:** Investigation, Funding acquisition. **Xiaoxia Yan:** Investigation. **Jinhua Wang:** Investigation, Supervision. **Liqiang Luo:** Conceptualization, Methodology, Investigation, Writing - review & editing, Supervision, Funding acquisition.

Declaration of competing interest

The authors declare that they have no known competing financial interests or personal relationships that could have appeared to influence the work reported in this paper.

Acknowledgments

This work was supported by the National Natural Science Foundation of China (Nos. 61571278, 61571280, 21974085, and 61971274).

Appendix A. Supplementary data

Supplementary data to this article can be found online at https://doi.org/10.1016/j.msec.2020.111443.

References

[1] Y. Shu, J. Xu, J. Chen, Q. Xu, X. Xiao, D. Jin, H. Pang, Ultrasensitive electrochemical detection of H_2O_2 in living cells based on ultrathin MnO_2 nanosheets, Sens. Actuators B Chem. 252 (2017) 72–78.
[2] H. Heli, J. Pishahang, Cobalt oxide nanoparticles anchored to multiwalled carbon nanotubes: synthesis and application for enhanced electrocatalytic reaction and highly sensitive nonenzymatic detection of hydrogen peroxide, Electrochim. Acta 123 (2014) 518–526.
[3] K. Yuan, Y. Ni, L. Zhang, Facile hydrothermal synthesis of polyhedral Fe_3O_4 nanocrystals, influencing factors and application in the electrochemical detection of H_2O_2, J. Alloys Compd. 532 (2012) 10–15.
[4] A.L. Sanati, H. Karimi-Maleh, A. Badiei, P. Biparva, A.A. Ensafi, A voltammetric sensor based on NiO/CNTs ionic liquid carbon paste electrode for determination of morphine in the presence of diclofenac, Mater. Sci. Eng. C 35 (2014) 379–385.
[5] T. Zhu, Y. Zhang, L.Q. Luo, X.L. Zhao, Facile fabrication of NiO-decorated double-layer single-walled carbon nanotube buckypaper for glucose detection, ACS Appl. Mater. Interfaces 11 (2019) 10856–10861.
[6] X.Q. Cheng, J. Zhang, H.C. Chang, L.Q. Luo, F.Q. Nie, X.J. Feng, High performance Cu/Cu_2O nanohybrid electrocatalyst for nonenzymatic glucose detection, J. Mater. Chem. B 4 (2016) 4652–4656.
[7] H. Begum, M. Ahmed, S. Jeon, A novel δ-MnO_2 with carbon nanotubes nanocomposites as enzyme-free sensor for hydrogen peroxide electrosensing, RSC Adv. 6 (2016) 50572–50580.
[8] S.J. Li, J.C. Zhang, J. Li, H.Y. Yang, J.J. Meng, B. Zhang, A 3D sandwich structured hybrid of gold nanoparticles decorated MnO_2/graphene-carbon nanotubes as high performance H_2O_2 sensors, Sens. Actuators B Chem. 260 (2018) 1–11.
[9] F.Y. Zeng, Y. Pan, Y. Yang, Q.L. Li, G.Y. Li, Z.H. Hou, G. Gu, Facile construction of Mn_3O_4-MnO_2 hetero-nanorods/graphene nanocomposite for highly sensitive electrochemical detection of hydrogen peroxide, Electrochim. Acta 196 (2016) 587–596.
[10] P. Si, X.C. Dong, P. Chen, D.H. Kim, A hierarchically structured composite of Mn_3O_4/3D graphene foam for flexible nonenzymatic biosensors, J. Mater. Chem. B 1 (2013) 110–115.
[11] H. Zhu, A. Sigdel, S. Zhang, D. Su, Z. Xi, Q. Li, S. Sun, Core/shell Au/MnO nanoparticles prepared through controlled oxidation of AuMn as an electrocatalyst for sensitive H_2O_2 detection, Angew. Chem. Int. Ed. 53 (2015) 12508–12512.
[12] L. Wang, K.L. Wu, B.B. Jiang, Z.X. Zhang, X.Z. Li, B. Zhang, J. Lv, J. Suan, C. Non-enzymatic electrochemical sensors for the detection of H_2O_2 based on Mn_3O_4 octahedron submicrostructures, Micro Nano Lett. 9 (2014) 736–740.
[13] H.Y. Song, H. Zhao, X.F. Zhang, Y.M. Xu, X.L. Cheng, S. Gao, L.H. Huo, A hollow urchin-like α-MnO_2 as an electrochemical sensor for hydrogen peroxide and dopamine with high selectivity and sensitivity, Microchim. Acta 186 (2019) 210.
[14] Z. Cai, D.M. Zhang, L.L. Gu, P. Liu, K. Ye, K. Cheng, D.X. Cao, G.L. Wang, MnO_2 nanosheets as a high-efficiency electrocatalyst for H_2O_2 reduction in alkaline medium, RSC Adv. 6 (2016) 2546–2551.
[15] Y. Zheng, T. Zhou, C. Zhang, J. Mao, H. Liu, Z. Guo, Boosted charge transfer in SnS/SnO_2 heterostructures: toward high rate capability for sodium-ion batteries, Angew. Chem. Int. Ed. 55 (2016) 3408–3413.
[16] X. Zhu, N.R. Monahan, Z. Gong, H. Zhu, K.W. Williams, C.A. Nelson, Charge transfer excitons at van der waals interfaces, J. Am. Chem. Soc. 137 (2015) 8313–8320.
[17] C. Huang, S. Wu, A.M. Sanchez, J.J. Peters, R. Beanland, J.S. Ross, P. Rivera, W. Yao, D.H. Cobden, X. Xu, Lateral heterojunctions within monolayer $MoSe_2$-WSe_2 semiconductors, Nat. Mater. 13 (2014) 1096–1101.
[18] K.K. Bera, M. Chakraborty, S.R. Chowdhury, A. Ray, S. Das, S.K. Bhattacharya, Significantly improved and synergistic effect of Pt-ZnO-Bi_2O_3 ternary hetero-junctions toward anode-catalytic oxidation of methanol in alkali, Electrochim. Acta 322 (2019) 134775.
[19] F.F. Wu, Y. Zhou, H. Zhang, R. Yuan, Y.Q. Chai, Electrochemiluminescence peptide-based biosensor with hetero-nanostructures as coreaction accelerator for the ultrasensitive determination of tryptase, Anal. Chem. 90 (2018) 2263–2270.
[20] R. Praveen, R. Ramaraj, Facile synthesis of hetero-nanostructured cuprous oxide-gold composite material for sensitive enzymeless glucose detection, J. Electroanal. Chem. 851 (2019) 113454.
[21] J. Kim, J.N. Heo, J.Y. Do, R.K. Chava, M. Kang, Electrochemical synergies of heterostructured Fe_2O_3-MnO catalyst for oxygen evolution reaction in alkaline water splitting, Nanomaterials 9 (2019) 1486.
[22] J. Park, H.J. Kim, A. Oh, T. Kwon, H. Baik, S.I. Choi, K. Lee, RuOx-decorated multimetallic hetero-nanocages as highly efficient electrocatalysts toward the methanol oxidation reaction, Nanoscale 10 (2018) 21178–21185.
[23] M. Asif, H. Wang, S. Dong, A. Aziz, G. Zhang, F. Xiao, Metal oxide intercalated layered double hydroxide nanosphere: with enhanced electrocatalyic activity towards H_2O_2 for biological applications, Sens. Actuators B Chem. 239 (2017) 243–252.
[24] S.G. Rhee, H_2O_2, a necessary evil for cell signaling, Science 312 (2006) 1882–1883.
[25] C.K.O.D. Silva-Rackov, W.A. Lawal, P.A. Nfodzo, M.M.G.R. Vianna, C.A.O.D. Nascimento, H. Choi, Degradation of PFOA by hydrogen peroxide and persulfate activated by iron-modified diatomite, Appl. Catal. B Environ. 192 (2016) 253–259.
[26] G. Son, D.H. Kim, J.S. Lee, H. Lee, Enhanced methylene blue oxidative removal by copper electrode-based plasma irradiation with the addition of hydrogen peroxide, Chemosphere 157 (2016) 271–275.
[27] D. Demirbüker, I. Arcan, F. Tokatli, A. Yemenicioglu, Effects of hot rehydration in the presence of hydrogen peroxide on microbial quality, texture, color, and antioxidant activity of cold-stored intermediate-moisture sun-dried figs, J. Food Sci. 70 (2010) 153–159.
[28] M.S. Haddadin, S.A. Ibrahim, R.K. Robinson, Preservation of raw milk by activation of the natural lactoperoxidase systems, Food Control 7 (1996) 149–152.
[29] M. Özkan, A.E.L. Kırca, B. Cemeroğlu, Effects of hydrogen peroxide on the stability of ascorbic acid during storage in various fruit juices, Food Chem. 88 (2005)

591–597.
[30] H. Pelicano, D. Carney, P. Huang, ROS stress in cancer cells and therapeutic implications, Drug Resist. Update 7 (2004) 97–110.
[31] Y. Chen, E. Mcmillanward, J. Kong, S.J. Israels, S.B. Gibson, Oxidative stress induces autophagic cell death independent of apoptosis in transformed and cancer cells, Cell Death Differ. 15 (2008) 171–182.
[32] E.R. Whittemore, D.T. Loo, J.A. Watt, C.W. Cotmans, A detailed analysis of hydrogen peroxide-induced cell death in primary neuronal culture, Neuroscience 67 (1995) 921–932.
[33] M. Yi, Z. Shen, A review on mechanical exfoliation for the scalable production of graphene, J. Mater. Chem. A 3 (2015) 11700–11715.
[34] T.S. Sreeprasad, V. Berry, How do the electrical properties of graphene change with its functionalization? Small 9 (2013) 341–350.
[35] M.J. Allen, V.C. Tung, R.B. Kaner, Honeycomb carbon: a review of graphene, Chem. Rev. 110 (2009) 132–145.
[36] S. Taniselass, M.K.M. Arshad, S.C.B. Gopinath, Current state of green reduction strategies: solution-processed reduced graphene oxide for healthcare biodetection, Mater. Sci. Eng. C 96 (2019) 904–914.
[37] V.H. Nguyen, C. Lamiel, D. Kharismadewi, V.C. Tran, J.J. Shim, Covalently bonded reduced graphene oxide/polyaniline composite for electrochemical sensors and capacitors, J. Electroanal. Chem. 758 (2015) 148–155.
[38] M.R. Mahmoudian, Y. Alias, W.J. Basirun, P.M. Woi, M. Sookhakian, Facile preparation of MnO_2 nanotubes/reduced graphene oxide nanocomposite for electrochemical sensing of hydrogen peroxide, Sens. Actuators B Chem. 201 (2014) 526–534.
[39] M. Wang, J.W. Ma, Q.B. Chang, X.B. Fan, G.L. Zhang, F.B. Zhang, W.C. Peng, Y. Li, Fabrication of a novel ZnO-CoO/rGO nanocomposite for nonenzymatic detection of glucose and hydrogen peroxide, Ceram. Int. 44 (2018) 5250–5256.
[40] Z.Y. Wang, S. Gao, T. Fei, S. Liu, T. Zhang, Construction of ZnO/SnO_2 heterostructure on reduced graphene oxide for enhanced nitrogen dioxide sensitive performances at room temperature, ACS Sensors 4 (2019) 2048–2057.
[41] N.N. Wang, X.J. Ma, H.Y. Xu, L. Chen, J. Yue, F.E. Niu, J. Yang, Y.T. Yang, Porous $ZnMn_2O_4$ microspheres as a promising anode material for advanced lithium-ion batteries, Nano Energy 6 (2014) 193–199.
[42] Y.Y. Li, K. Huan, D.M. Deng, L. Tang, J.H. Wang, L.Q. Luo, Facile synthesis of $ZnMn_2O_4$@rGO microspheres for ultrasensitive electrochemical detection of hydrogen peroxide from human breast cancer cells, ACS Appl. Mater. Interfaces 12 (2020) 3430–3437.
[43] H. Begum, M.S. Ahmed, S. Jeon, A novel delta-MnO_2 with carbon nanotubes nanocomposite as an enzyme-free sensor for hydrogen peroxide electrosensing, RSC Adv. 6 (2016) 50572–50580.
[44] S.Y. Liu, J. Xie, Y.X. Zheng, G.S. Cao, T.J. Zhu, X.B. Zhao, Nanocrystal manganese oxide (Mn_3O_4, MnO) anchored on graphite nanosheet with improved electrochemical Li-storage properties, Electrochim. Acta 66 (2012) 271–278.
[45] L. Na, Z. Geng, M. Cao, L. Ren, X. Zhao, B. Liu, T. Yuan, C. Hu, Well-dispersed ultrafine Mn_3O_4 nanoparticles on graphene as a promising catalyst for the thermal decomposition of ammonium perchlorate, Carbon 54 (2013) 124–132.
[46] X. Li, Y. Zhu, X. Zhang, J. Liang, Y. Qian, MnO@1-D carbon composites from the precursor $C_4H_4MnO_6$ and their high-performance in lithium batteries, RSC Adv. 3 (2013) 10001–10006.
[47] L.Z. Sheng, H. Jiang, S.P. Liu, M.H. Chen, T. Wei, Z.J. Fan, Nitrogen-doped carbon-coated MnO nanoparticles anchored on interconnected graphene ribbons for high-performance lithium-ion batteries, J. Power Sources 397 (2018) 325–333.
[48] Y. Sun, X. Hu, W. Luo, F. Xia, Y. Huang, Reconstruction of conformal nanoscale MnO on graphene as a high-capacity and long-life anode material for lithium ion batteries, Adv. Funct. Mater. 23 (2013) 2436-2344.
[49] J. Zhang, R.X. Chu, Y.L. Chen, Y.B. Zeng, Y. Zhang, H. Guo, Porous carbon encapsulated Mn_3O_4 for stable lithium storage and its ex-situ XPS study, Electrochim. Acta 319 (2019) 518–526.
[50] L. Wang, Y. Li, Z. Han, L. Chen, B. Qian, X. Jiang, J. Pinto, G. Yang, Composite structure and properties of Mn_3O_4/graphene oxide and Mn_3O_4/graphene, J. Mater. Chem. A 1 (2013) 8385–8397.
[51] H. Xia, Y. Wan, F. Yan, L. Lu, Manganese oxide thin films prepared by pulsed laser deposition for thin film microbatteries, Mater. Chem. Phys. 143 (2014) 720–727.
[52] Y. Chu, L. Guo, B. Xi, Z. Feng, F. Wu, Y. Lin, J. Liu, D. Sun, J. Feng, Y. Qian, Embedding MnO@Mn_3O_4 nanoparticles in an N-doped-carbon framework derived from Mn-organic clusters for efficient lithium storage, Adv. Mater. 30 (2018) 1704244.
[53] M. Chigane, M. Ishikawa, Manganese oxide thin film preparation by potentiostatic electrolyses and electrochromism, J. Electrochem. Soc. 147 (2000) 2246–2251.
[54] E. Samuel, H.S. Jo, B. Joshi, H.G. Park, Y.I. Kim, S. An, M.T. Swihart, J.M. Yun, K.H. Kim, S.S. Yoon, High-performance supercapacitors using flexible and free-standing MnO_x/carbamide carbon nanofibers, Appl. Surf. Sci. 423 (2017) 210–218.
[55] B. Mayer, S. Uhlenbrock, M. Neumann, XPS satellites in transition metal oxides, J. Electron Spectrosc. Relat. Phenom. 81 (1996) 63–67.
[56] R.J. Iwanowski, M.H. Heinonen, E. Janik, X-ray photoelectron spectra of zinc-blende MnTe, Chem. Phys. Lett. 387 (2004) 110–115.
[57] L. Yin, I. Adler, T. Tsang, L.J. Matienzo, S.O. Grim, Paramagnetism and shake-up satellites in X-ray photoelectron spectra, Chem. Phys. Lett. 24 (1974) 81–84.
[58] B.G. Peng, J.W. Cui, Y. Wang, J.Q. Liu, H.M. Zheng, L. Jin, X.Y. Zhang, Y. Zhang, Y.C. Wu, CeO_{2-x}/C/rGO nanocomposites derived from Ce-MOF and graphene oxide as a robust platform for highly sensitive uric acid detection, Nanoscale 10 (2018) 1939–1945.
[59] Y. Fan, Z.Y. Zhou, Y. Feng, Y. Zhou, L. Wen, K.M. Shih, Degradation mechanisms of ofloxacin and cefazolin using peroxymonosulfate activated by reduced graphene oxide-$CoFe_2O_4$ composites, Chem. Eng. J. 383 (2020) 123056.
[60] X.Y. Qi, K.Y. Pu, H. Li, X.Z. Zhou, S.X. Wu, Q.L. Fan, B. Liu, F. Boey, W. Huang, H. Zhang, Amphiphilic graphene composites, Angew. Chem. Int. Ed. 49 (2010) 9426–9429.
[61] Y. Zhang, S. Liu, Y. Li, D. Deng, X. Si, Y. Ding, H. He, L. Luo, Z. Wang, Electrospun graphene decorated $MnCo_2O_4$ composite nanofibers for glucose biosensing, Biosens. Bioelectron. 66 (2015) 308–315.
[62] S. Guan, X. Fu, Z. Lao, C. Jin, Z. Peng, NiS-MoS_2 hetero-nanosheet arrays electrocatalysts for efficient overall water splitting, Sustain. Energy Fuels 3 (2019) 2056–2066.
[63] J.M. Suh, W. Sohn, Y.S. Shim, J.S. Choi, Y.G. Song, T.L. Kim, J.M. Jeon, K.C. Kwon, K.S. Choi, C.Y. Kang, H.G. Byun, H.W. Jang, P-P heterojunction of nickel oxide decorated cobalt oxide nanorods for enhanced sensitivity and selectivity toward volatile organic compounds, ACS Appl. Mater. Interfaces 10 (2018) 1050–1058.
[64] X.X. Chang, T. Wang, P. Zhang, J.J. Zhang, A. Li, J.L. Gong, Enhanced surface reaction kinetics and charge separation of p-n heterojunction Co_3O_4/$BiVO_4$ photoanodes, J. Am. Chem. Soc. 137 (2015) 8356–8359.
[65] M. Liu, S. He, W. Chen, Co_3O_4 nanowires supported on 3D N-doped carbon foam as an electrochemical sensing platform for efficient H_2O_2 detection, Nanoscale 6 (2014) 11769–11776.
[66] M. Liu, R. Liu, W. Chen, Graphene wrapped Cu_2O nanocubes: non-enzymatic electrochemical sensors for the detection of glucose and hydrogen peroxide with enhanced stability, Biosens. Bioelectron. 45 (2013) 206–212.
[67] X. Ke, G. Zhu, Y. Dai, Y. Shen, J. Yang, J. Liu, Fabrication of Pt-ZnO composite nanotube modified electrodes for the detection of H_2O_2, J. Electroanal. Chem. 817 (2018) 176–183.
[68] M. Wang, J. Ma, X. Guan, W. Peng, X. Fan, G. Zhang, F. Zhang, Y. Li, A novel H_2O_2 electrochemical sensor based on $NiCo_2S_4$ functionalized reduced graphene oxide, J. Alloys Compd. 784 (2019) 827–833.
[69] X. Zhao, Z. Li, C. Chen, Y. Wu, Z. Zhu, H. Zhao, M. Lan, A novel biomimetic hydrogen peroxide biosensor based on Pt flowers-decorated Fe_3O_4/graphene nanocomposite, Electroanalysis 29 (2017) 1518–1523.
[70] K. Vasuki, K.J. Babu, S. Sheet, G. Siva, A.R. Kim, D.J. Yoo, Amperometric hydrogen peroxide sensor based on the use of $CoFe_2O_4$ hollow nanostructures, Microchim. Acta 184 (2017) 2579–2586.
[71] D.S. achari, C. Santhosh, R. Deivasegamani, R. Nivetha, A. Bhatnagar, S.K. Jeong, A. N. Grace, A non-enzymatic sensor for hydrogen peroxide based on the use of α-Fe_2O_3 nanoparticles deposited on the surface of NiO nanosheets, Microchim. Acta 184 (2017) 3223–3229.
[72] T. Liu, Y. Guo, Z. Zhang, Z. Miao, X. Zhang, Z. Su, Fabrication of hollow CuO/PANI hybrid nanofibers for non-enzymatic electrochemical detection of H_2O_2 and glucose, Sens. Actuators B Chem. 286 (2019) 370–376.
[73] S.J. Li, Y. Xing, H.Y. Yang, J.Y Huang, W.T. Wang, R.T. Liu, Electrochemical synthesis of a binary Mn-Co oxides decorated graphene nanocomposites for application in nonenzymatic H_2O_2 sensing, Int. J. Electrochem. Soc. 12 (2017) 6566–6576.